Journal of Molecular Liquids 404 (2024) 124851

Contents lists available at ScienceDirect

Journal of Molecular Liquids

journal homepage: www.elsevier.com/locate/molliq

Densities and isobaric heat capacities at high pressures of aqueous solutions of 2-diethylaminoethanol (DEAE) or 2-ethylaminoethanol (EAE) for CO_2 capture

Yisel Pérez-Milian, Alejandro Moreau, Juan D. Arroyave, Fredy Vélez, Xavier Paredes, David Vega-Maza *

TermoCal Research Group, Research Institute On Bioeconomy, University of Valladolid, Paseo del Cauce 59, 47011 Valladolid, Spain

ARTICLE INFO

Keywords:
Isobaric heat capacity
Density
High pressure
DEAE + H_2O
EAE + H_2O

ABSTRACT

Densities and isobaric heat capacities of DEAE + H_2O and EAE + H_2O systems are presented in this paper. Density measurements were carried out at high pressure (up to 100 MPa) and temperatures from (293.15 to 393.15) K, with amine mass fractions of 0.1; 0.2; 0.3 and 0.4. These data were gathered using a vibrating tube densimeter (Anton Paar DMA HPM) with a relative expanded uncertainty of ±0.1 % ($k = 2$). A non-adiabatic quasi-isothermal flow calorimeter was used for isobaric heat capacity measurements with a relative expanded uncertainty better than 1 % ($k = 2$). Measurements reached pressures up to 25 MPa, and temperatures from (293.15 to 353.15) K, with amine mass fractions of 0.1; 0.2; 0.3 and 0.4. Both amine DEAE + H_2O and EAE + H_2O systems show a density and isobaric heat capacity decrease with amine mass fraction increase. Density data as a function of temperature, pressure and molality were fitted using a modified Tammann-Tait empirical equation of state. Furthermore, isobaric heat capacity data were correlated using an empirical function of temperature and amine mass fraction, but not pressure due to its lack of sensitivity in the measured data. Both correlations are in good agreement with the uncertainties. Comparison with experimental density data available in literature showed lower deviations than the associated uncertainties. Our isobaric heat capacity experimental data agree well with the scarce literature.

1. Introduction

Human activities have led to a substantial increase in carbon emissions over the last 150 years, causing a progressive rise in global surface temperature at a rate unprecedented in at least the last 2000 years [1]. Renewable energies, energy efficiency, energy carrier switching, and carbon capture, utilization, and storage (CCUS) are attractive technology mitigation strategies [2–4].

Amine-based carbon dioxide (CO_2) capture is a well-established and widely used gas separation technology. While low temperature and high pressure provide the most favorable conditions for absorption [5,6], post-combustion carbon capture typically operates at atmospheric pressure [7,8]. Consequently, experimental data for the mixtures involved under high-pressure conditions are scarce in the literature. However, amine-based gas separation technology is also employed for large-scale purification of gases like gas sweetening, where CO_2 and H_2S are removed. Gas sweetening utilizes high-pressure amine absorption [4]. Notable examples include the Khurmala field in Iraqi Kurdistan, employing an absorption pressure of 7 MPa, and the Sulfa-Check project in California, operating at 4 MPa [9,10]. Either way, thermophysical properties such as density and isobaric heat capacity for amine aqueous solutions across a wide range of pressures, concentrations, and temperatures remain largely absent in the literature, hindering the optimization of these processes [11]. In this regard, density is essential in the design of equipment and optimization of gas treatment processes, in the CO_2 solubility modeling, and in the reaction kinetics involved in CO_2 capture. Moreover, accurate isobaric heat capacity is essential for designing energy-efficient systems [12,13]. Both properties are key to complete a comprehensive thermodynamic characterization of those mixtures and increase our knowledge about the molecular interactions in them, hence improve predictive models.

Monoethanolamine (MEA), a primary amine, is the benchmark solvent used in the amine-based CO_2 capture process, with a good absorption capacity, high reactivity with CO_2 and proven stability [14].

* Corresponding author.
E-mail address: david.vega@uva.es (D. Vega-Maza).

https://doi.org/10.1016/j.molliq.2024.124851
Received 5 February 2024; Received in revised form 24 April 2024; Accepted 26 April 2024
Available online 27 April 2024

Table 1
Material description.

Compound	CAS Number	Source	Mass fraction purity[a]	Purification method
DEAE	100–37-8	Sigma-Aldrich	≥ 0.995	None
EAE	110–73-6	Sigma-Aldrich	≥ 0.98	None
Water	7732–18-5	Sigma-Aldrich	conductivity ≤ $2{\cdot}10^{-6}$ $\Omega^{-1}{\cdot}cm^{-1}$	None

[a] As stated by the supplier by gas chromatography.

Despite this, primary and secondary amines show some drawbacks in comparison with tertiary amines, such as higher enthalpy of absorption, lower CO_2 loading capacities, higher susceptibility to oxidation and thermal degradation in the regeneration process [13,15]. Hindered secondary amines can also show higher CO_2 loading capacities and lower enthalpy of absorption, tertiaries alike [16]. A low enthalpy of absorption implies a reduction in the energy load required by the amine scrubbing separation process, hence reducing the energy penalty and increasing the efficiency. However, newly proposed amines and their blends lack thermophysical data and models that would assess their performance against currently used solvents. This work is part of our effort aimed at filling these data gaps in different properties and conditions of operation.

In this study, we focused on two amines with a similar structure: 2-diethylaminoethanol (DEAE), a tertiary ethanolamine, and 2-ethylaminoethanol (EAE), a secondary ethanolamine. CO_2 absorption into aqueous solutions of DEAE or EAE has been studied by [17], yielding very promising results. At 30 % of amine mass percent and 313.15 K, DEAE + H_2O and EAE + H_2O mixtures exhibited a high CO_2 loading, exceeding 0.65 mol-CO_2/mol-amine, and a low enthalpy of absorption, approximately 70 kJ/mol-CO_2. In comparison, under the same conditions of amine mass percent and temperature, MEA aqueous solution presented a CO_2 loading of 0.59 mol-CO_2/mol-amine and an enthalpy of absorption of 85.13 kJ/mol-CO_2. Furthermore, EAE + H_2O shows reaction kinetics very similar to those of MEA + H_2O. These features make them competitive candidates for amine-based CO_2 capture.

The main objective of this study is to measure density and isobaric heat capacity of DEAE + H_2O and EAE + H_2O at amine mass fractions from 0.1 to 0.4, over a wide range of temperatures and pressures. Density measurements were performed with a vibrating tube densimeter with a relative expanded uncertainty ($k = 2$) of ±0.1 % at six different temperatures from (293.15 to 393.15) K and pressure up to 100 MPa. For isobaric heat capacity, a non-adiabatic quasi-isothermal flow calorimeter was used at four different temperatures from (293.15 to 353.15) K and pressure up to 25 MPa, with a relative expanded uncertainty ($k = 2$) better than 1 %. We found two data sets in the literature reporting density data in EAE + H_2O systems, and two data sets reporting density data in DEAE + H_2O systems, although the four of them are only at ambient pressure. Our search for comparable isobaric heat capacity data yielded only one relevant reference. Despite limited literature data, the available references provided an adequate comparison point for our results.

2. Experimental

2.1. Materials

2-Diethylaminoethanol (DEAE) and 2-ethylaminoethanol (EAE) samples were purchased from Sigma-Aldrich and their features are detailed in Table 1. Water was used for densimeter calibration and solution preparation. Aqueous amine solutions were prepared using an analytical balance (Radwag scale model PS750/C/2) with a resolution of 1 mg. The expanded uncertainty of the amine mass fraction is 0.0004 at 95.5 % confidence. Immediately upon preparation, aqueous amine solutions were degassed using a water-filled ultrasonic bath (Branson 3210). To minimize potential CO_2 absorption from the air, the solutions were stored in the dark within glass bottles sealed with both a lid and a film to prevent contamination. The time between preparation and measurement was kept to a maximum of two days. The stability of the solutions was monitored through *p*H measurements, utilizing a Mettler Toledo FiveEasy Plus pH meter.

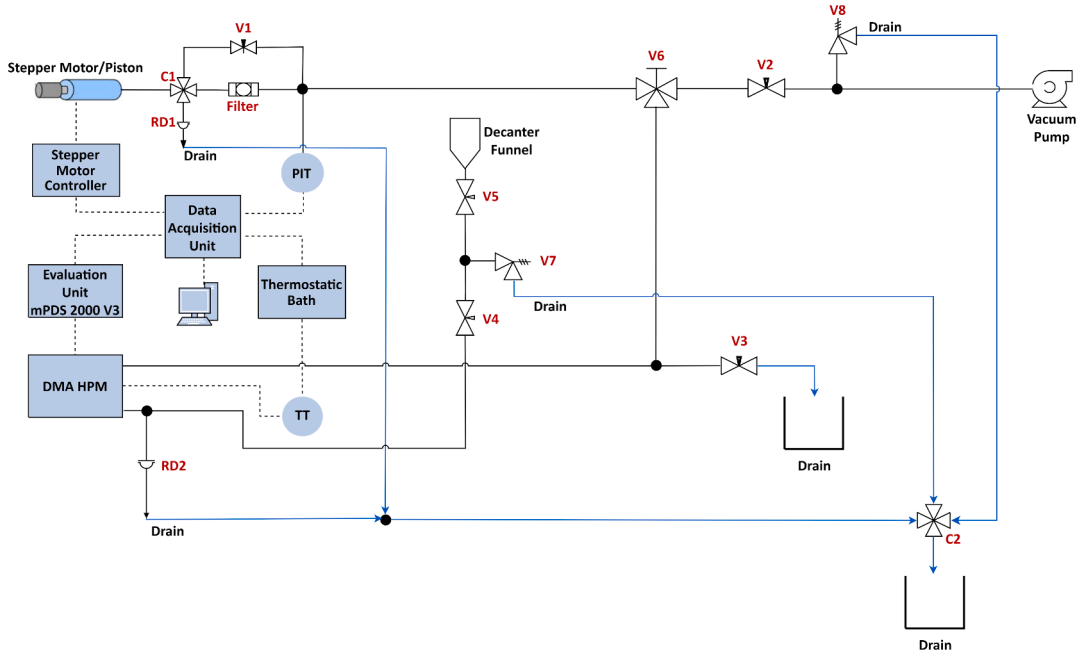

Fig. 1. Scheme of vibrating tube densimeter (TermoCal laboratory). PIT: pressure indicator and transmitter Druck DPI; TT: Temperature transmitter Pt100; V1-V5: high-pressure needle valves; V6: high-pressure three-way valve; V7 and V8: relief valves; RD: rupture disc; C1 and C2: crosses.

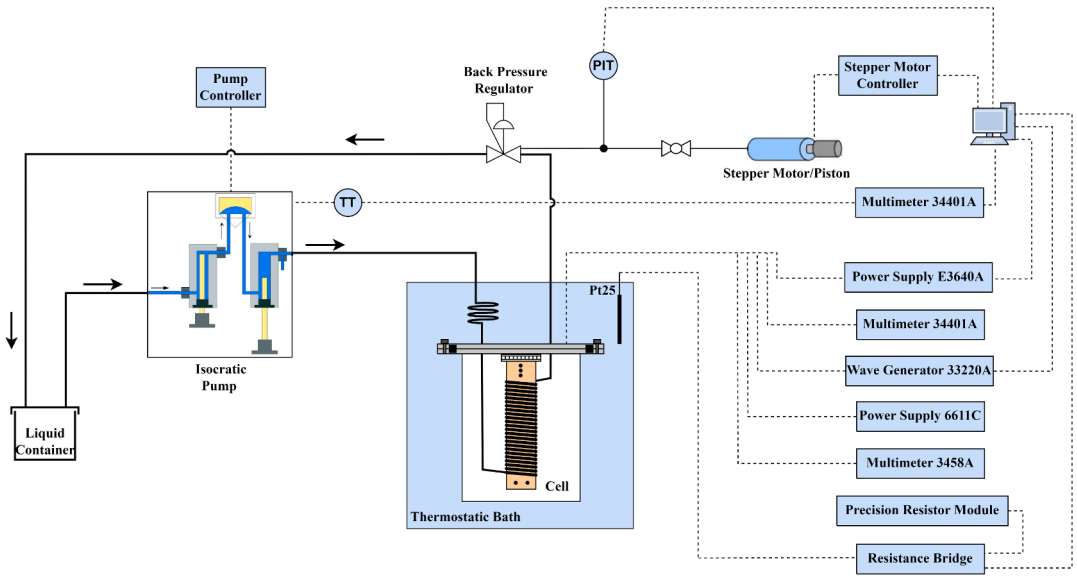

Fig. 2. Scheme of flow calorimeter (TermoCal laboratory). PIT: pressure indicator and transmitter Druck DPI; TT: Temperature transmitter Pt100.

2.2. Apparatus and procedure

2.2.1. Density measurements

A vibrating tube densimeter (Anton Paar DMA HPM) was used for density, ρ, measurement. The working principle is based on the electromagnetic excitation of a U-shaped tube which contains a fluid, whereby the oscillation period of the fundamental bending mode of the tube is correlated to the density of the fluid. The periods were measured using an mPDS 2000 V3 evaluation unit, with 10^{-6} ms standard uncertainty over periods around 2.6 ms. The employed method measured densities from (0 to 3000) kg·m^{-3}, with a resolution of 10^{-2} kg·m^{-3}. Temperature in the densimeter was measured with a Pt100 probe calibrated with an expanded uncertainty of 0.02 K. Pressure expanded uncertainty was 0.02 MPa. All expanded uncertainties define intervals having a level of confidence of 95.5 %. The apparatus works in a fully automated fashion, controlled by code implemented in Agilent VEE Pro software. Fig. 1 shows a schematic description of the equipment used. The measuring procedure can be found in our earlier work [18].

Following the method described in [19] developed by [20] and modified by [21], the densimeter was calibrated using water and vacuum over the whole working temperature and pressure ranges, i.e., at temperature from (293.15 to 393.15) K and pressure up to 100 MPa. The vibrating period, τ, can be related to the density of the fluid using Equation (1) proposed by [20].

$$\rho(T,p) = A(T)\tau^2(T,p) - B(T,p) \tag{1}$$

where $A(T)$ and $B(T,p)$ are two characteristic parameters of the apparatus, which can be determined by a set-up calibration at each temperature and pressure. For these parameters Equations (2) and 3, suggested by [20,21], were used:

$$A(T) = \frac{\rho_{ref}(T, 0.1\text{MPa})}{\tau^2_{\text{ref}}(T, 0.1\text{MPa}) - \tau^2_{\text{vacuum}}(T)} \tag{2}$$

$$B(T,p) = \frac{\rho_{\text{ref}}(T, 0.1\text{MPa})}{\tau^2_{\text{ref}}(T, 0.1\text{MPa}) - \tau^2_{\text{vacuum}}(T)}\tau^2_{\text{ref}}(T,p) - \rho_{\text{ref}}(T,p) \tag{3}$$

where the subscript *"ref"* indicates a fluid with a well-known density; in this case, water. These equations are utilized over the temperature and pressure interval of study.

Equation (2) adopts the assumption from Lagourette et al. [20] and followed by Lugo et al. [22] that parameter $A(T)$ is independent of pressure, with only $B(T, p)$ exhibiting significant pressure dependence. It assumes that the pressure dependence of the elastic constant of the tube compensates the dependence of the internal volume of the tube on $A(T)$. This assumption introduces negligible error due to the observed similarity between the measured densities and those of water.

Uncertainty calculations for density measurement were carried out following the procedure described in the Guide to the Expression of Uncertainty in Measurement [23] and explained in [19], obtaining a relative expanded uncertainty (U_r) of ±0.1 % in the density values with coverage factor $k = 2$ for 95.5 % level of confidence.

2.2.2. Isobaric heat capacities

A non-adiabatic quasi-isothermal flow calorimeter was used for the isobaric heat capacity measurements. The relative expanded uncertainty was better than 1 % with coverage factor $k = 2$ for a 95.5 % level of confidence. The detailed uncertainty analysis was given earlier [24,25].

The working principle of the flow calorimeter is based on a fluid circulating at a constant flow rate through a calorimetric cell. Simultaneous heating and cooling take place within the cell to maintain a fixed temperature difference of 0.5 K between the inlet and outlet temperatures with an uncertainty of 0.01 K. A schematic view of the calorimeter is shown in Fig. 2. Five different flows between (0.9 and 1.45) mL·min^{-1} were set, finding that the isobaric heat capacity measurements were independent of the flow. This range has been proven in [25] to be the optimum for aqueous solutions of amines.

Net power exchange ($\dot{Q}_{net}$) can be related to the isobaric heat capacity (c_p) as it is shown in Equation (4), over the working range of temperature and pressure.

$$c_p = \frac{\dot{Q}_{net}}{\dot{m}\Delta T} = \frac{\dot{Q}_{net}}{\dot{v}\rho\Delta T} \tag{4}$$

where $\dot{m}$ is the mass flow. It is determined using the volumetric flow, $\dot{v}$, set in the isocratic pump and the density of the fluid at the pump (pressure and temperature) conditions. Experimental density, ρ, data was also measured with a vibrating tube densimeter previously described. These new data are also reported in this study. Net power exchange ($\dot{Q}_{net}$) was calculated as a linear function that correlated the difference between the calorific power measurement without flow ($\dot{Q}_{base}$) and with flow ($\dot{Q}_{measured}$), as is shown in Equation (5).

Table 2
Experimental densities, ρ, for DEAE(1) + H_2O(2) mixtures at different conditions of temperature, T, pressure, p, amine mass fraction, w_1, and equivalent amine molality, b_1.[a]

	ρ/(kg·m^{-3})					
	T/K					
p/MPa	293.15	313.15	333.15	353.15	373.15	393.15
	$w_1 = 0.100$ ($b_1 = 0.948$ mol·kg^{-1})					
0.1	995.2	987.9	977.4	964.9		
0.5	995.3	988.1	977.6	965.1		
1	995.5	988.2	977.8	965.3	950.7	934.4
2	995.8	988.6	978.3	965.7	951.2	935.0
5	997.1	989.9	979.6	967.1	952.7	936.6
10	999.1	991.9	981.7	969.3	954.9	939.1
15	1001.2	993.9	983.7	971.4	957.3	941.6
20	1003.2	995.9	985.7	973.6	959.5	944.1
30	1007.1	999.8	989.7	977.7	964.0	948.8
40	1010.9	1003.6	993.7	981.8	968.3	953.4
50	1014.7	1007.4	997.5	985.8	972.5	957.9
60	1018.4	1011.0	1001.2	989.6	976.5	962.3
70	1022.1	1014.7	1004.9	993.5	980.5	966.5
80	1025.7	1018.2	1008.5	997.2	984.5	970.6
90	1029.3	1021.7	1012.1	1000.9	988.2	974.6
100	1032.8	1025.2	1015.6	1004.4	992.0	978.5
	$w_1 = 0.200$ ($b_1 = 2.133$ mol·kg^{-1})					
0.1	993.1	983.2	970.7	956.4		
0.5	993.2	983.4	970.9	956.6		
1	993.4	983.5	971.1	956.8	940.8	923.2
2	993.7	983.9	971.5	957.3	941.3	923.8
5	994.9	985.2	972.9	958.7	942.8	925.5
10	996.8	987.1	975.0	961.0	945.3	928.2
15	998.7	989.1	977.1	963.2	947.7	930.9
20	1000.6	991.1	979.1	965.4	950.1	933.5
30	1004.2	994.9	983.1	969.7	954.7	938.5
40	1007.8	998.6	987.1	973.8	959.2	943.3
50	1011.4	1002.2	990.9	977.9	963.5	948.0
60	1014.9	1005.8	994.6	981.8	967.7	952.6
70	1018.3	1009.3	998.2	985.7	971.7	956.9
80	1021.6	1012.7	1001.8	989.4	975.7	961.1
90	1024.9	1016.1	1005.3	993.1	979.6	965.3
100	1028.2	1019.4	1008.7	996.6	983.3	969.3
	$w_1 = 0.300$ ($b_1 = 3.657$ mol·kg^{-1})					
0.1	989.5	976.8	962.2	946.4		
0.5	989.6	976.9	962.4	946.6		
1	989.7	977.1	962.6	946.8	929.2	910.4
2	990.1	977.5	963.1	947.3	929.7	911.0
5	991.3	978.8	964.5	948.8	931.4	912.9
10	993.2	980.8	966.7	951.2	934.0	915.9
15	995.1	982.8	968.9	953.6	936.7	918.8
20	997.0	984.8	971.0	955.9	939.2	921.6
30	1000.6	988.7	975.2	960.3	944.2	927.0
40	1004.1	992.4	979.2	964.8	948.9	932.2
50	1007.6	996.1	983.1	969.0	953.4	937.1
60	1011.0	999.7	986.9	973.0	957.8	941.9
70	1014.4	1003.2	990.6	977.0	962.0	946.5
80	1017.7	1006.6	994.2	980.8	966.2	951.0
90	1020.9	1010.0	997.7	984.5	970.2	955.2
100	1024.0	1013.2	1001.2	988.1	974.1	959.4
	$w_1 = 0.400$ ($b_1 = 5.689$ mol·kg^{-1})					
0.1	983.1	968.5	952.3	934.9		
0.5	983.2	968.6	952.5	935.1		
1	983.4	968.8	952.8	935.4	916.7	896.8
2	983.8	969.2	953.2	935.9	917.3	897.5
5	985.0	970.6	954.7	937.5	919.1	899.6
10	987.0	972.7	957.1	940.1	921.9	902.8
15	988.9	974.7	959.4	942.7	924.8	906.0
20	990.9	976.9	961.6	945.2	927.6	909.0
30	994.6	980.9	966.0	949.9	932.8	914.9
40	998.3	984.7	970.2	954.5	937.8	920.5
50	1001.8	988.5	974.3	958.9	942.6	925.7
60	1005.3	992.2	978.2	963.2	947.2	930.7
70	1008.6	995.8	982.0	967.3	951.6	935.5
80	1012.0	999.2	985.7	971.2	956.0	940.2
90	1015.1	1002.6	989.3	975.1	960.1	944.6
100	1018.3	1006.0	992.8	978.8	964.1	949.0

[a] Expanded uncertainties ($k = 2$): $U(T) = 0.02$ K; $U_r(p) = 0.0002$; $U_r(w) = 0.0004$ and $U(\rho) = 0.7$ kg·m^{-3}.

Table 3
Experimental densities, ρ, for EAE(1) + H_2O(2) mixture at different conditions of temperature, T, pressure, p, amine mass fraction, w_1, and equivalent amine molality, b_1.[a]

	ρ/(kg·m^{-3})					
	T/K					
p/MPa	293.15	313.15	333.15	353.15	373.15	393.15
	$w_1 = 0.100$ ($b_1 = 1.246$ mol·kg^{-1})					
0.1	995.6	988.6	978.5	966.4		
0.5	995.6	988.7	978.7	966.5		
1	995.8	988.8	978.9	966.7	952.6	936.9
2	996.1	989.3	979.3	967.2	953.1	937.4
5	997.4	990.5	980.6	968.5	954.6	939.0
10	999.4	992.5	982.7	970.7	956.8	941.4
15	1001.5	994.5	984.8	972.8	959.1	943.9
20	1003.5	996.5	986.8	975.0	961.3	946.3
30	1007.5	1000.4	990.7	979.1	965.8	951.0
40	1011.3	1004.3	994.7	983.2	970.0	955.5
50	1015.1	1008.0	998.5	987.1	974.1	959.9
60	1018.9	1011.7	1002.2	990.9	978.1	964.3
70	1022.6	1015.3	1005.9	994.8	982.1	968.3
80	1026.2	1018.9	1009.5	998.4	986.0	972.5
90	1029.8	1022.4	1013.0	1002.1	989.7	976.4
100	1033.3	1025.9	1016.5	1005.6	993.4	980.3
	$w_1 = 0.200$ ($b_1 = 2.805$ mol·kg^{-1})					
0.1	995.3	986.4	974.6	961.3		
0.5	995.3	986.4	974.8	961.4		
1	995.5	986.5	975.0	961.5	946.4	929.8
2	995.8	986.9	975.4	962.0	946.9	930.3
5	997.0	988.1	976.7	963.4	948.3	931.9
10	998.9	990.0	978.8	965.5	950.7	934.5
15	1000.8	991.9	980.7	967.6	953.0	936.9
20	1002.6	993.8	982.7	969.7	955.2	939.4
30	1006.2	997.5	986.6	973.9	959.7	944.2
40	1009.8	1001.2	990.5	977.9	963.9	948.8
50	1013.3	1004.8	994.2	981.9	968.1	953.3
60	1016.8	1008.3	997.8	985.7	972.2	957.7
70	1020.2	1011.8	1001.4	989.4	976.1	961.9
80	1023.5	1015.2	1004.9	993.0	980.1	965.9
90	1026.8	1018.5	1008.4	996.6	983.7	969.9
100	1030.1	1021.8	1011.7	1000.1	987.4	973.9
	$w_1 = 0.300$ ($b_1 = 4.808$ mol·kg^{-1})					
0.1	995.2	983.6	970.1	955.4		
0.5	995.2	983.7	970.3	955.5		
1	995.3	983.8	970.5	955.7	939.5	921.9
2	995.6	984.2	970.9	956.2	940.0	922.6
5	996.8	985.4	972.1	957.5	941.5	924.2
10	998.6	987.3	974.3	959.8	943.9	926.8
15	1000.4	989.1	976.3	961.9	946.3	929.5
20	1002.1	991.0	978.2	964.2	948.6	932.1
30	1005.6	994.7	982.1	968.2	953.2	937.0
40	1009.0	998.3	986.0	972.4	957.5	941.8
50	1012.3	1001.8	989.7	976.3	961.8	946.4
60	1015.6	1005.2	993.3	980.1	965.9	950.9
70	1018.8	1008.6	996.8	983.9	969.9	955.1
80	1022.0	1011.9	1000.3	987.6	973.7	959.3
90	1025.1	1015.1	1003.7	991.1	977.6	963.4
100	1028.2	1018.3	1007.0	994.6	981.3	967.3
	$w_1 = 0.400$ ($b_1 = 7.484$ mol·kg^{-1})					
0.1	993.1	979.4	964.3	948.5		
0.5	993.2	979.5	964.5	948.6		
1	993.3	979.7	964.7	948.8	931.7	913.5
2	993.6	980.1	965.2	949.3	932.3	914.1
5	994.8	981.2	966.5	950.7	933.8	915.9
10	996.6	983.2	968.6	953.0	936.3	918.7
15	998.4	985.1	970.7	955.3	938.8	921.4
20	1000.2	987.0	972.8	957.6	941.2	924.1
30	1003.7	990.7	976.7	961.8	946.0	929.3
40	1007.1	994.3	980.6	966.0	950.5	934.2
50	1010.4	997.8	984.4	970.1	954.9	939.0
60	1013.6	1001.3	988.1	973.9	959.1	943.6
70	1016.8	1004.7	991.6	977.8	963.2	948.0
80	1020.0	1008.0	995.1	981.5	967.2	952.3
90	1023.0	1011.2	998.5	985.1	971.0	956.4
100	1026.0	1014.3	1001.9	988.6	974.8	960.4

[a] Expanded uncertainties ($k = 2$): $U(T) = 0.02$ K; $U_r(p) = 0.0002$; $U_r(w) = 0.0004$ and $U(\rho) = 0.7$ kg·m^{-3}.

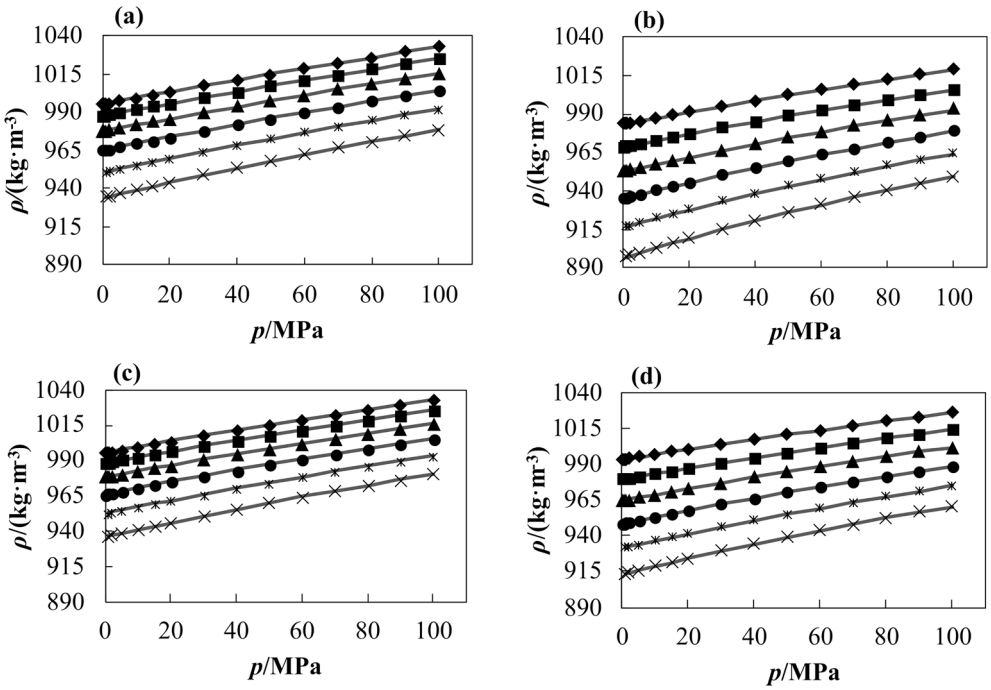

Fig. 3. Experimental density, ρ, as a function of pressure, p. Mixtures: DEAE + H_2O at amine mass fraction: a) $w_{DEAE} = 0.1$; b) $w_{DEAE} = 0.4$ and, EAE + H_2O at amine mass fraction: c) $w_{EAE} = 0.1$; d) $w_{EAE} = 0.4$. Isotherms: (◆) 293.15 K; (■) 313.15 K; (▲) 333.15 K; (●) 353.15 K; (*) 373.15 K and (×) 393.15 K. Lines represent the calculated values using modified Tammann-Tait (Equations 9 to 12) with the parameters given in Table 5.

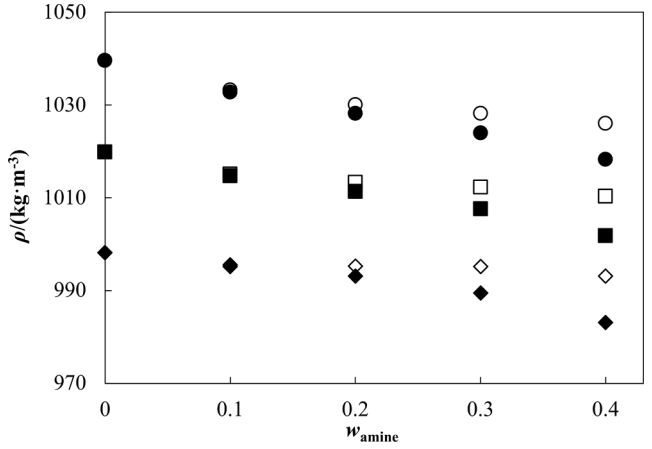

Fig. 4. Experimental density, ρ, as a function of amine mass fraction, w_{amine}, at a temperature of 293.15 K. Filled symbols: DEAE + H_2O. Empty symbols: EAE + H_2O. Pressures: (diamond) $p = 0.1$ MPa; (square) $p = 50$ MPa and (circle) $p = 100$ MPa. Data for water ($w_{amine} = 0$) from NIST REFPROP database [34].

Table 4
Coefficients β_{0j}, and γ_0 for pure water (molality $b_1 = 0$ mol·kg^{-1}) in Equations (11) and (12).

β_{00}	β_{01}	β_{02}	β_{03}	γ_0
-2894.13	16489.61	-27612.67	14807.00	0.13265

$$\dot{Q}_{net} = a + b\left(\dot{Q}_{base} - \dot{Q}_{measured}\right) \quad (5)$$

where a and b are two parameters determined in a thermal calibration experiment with a fluid of well-known isobaric heat capacity. Water was used for the calibration procedure.

Table 5
Coefficients α_{ij}, β_{ij}, and γ_i, and absolute average relative deviation (AAD), average relative deviation (Bias), maximum absolute relative deviation (MAD) and standard deviation (σ) in Equations 9 to 12.

Parameters	Systems	
	DEAE + H_2O	EAE + H_2O
α_{10}	2813.7743	2727.7136
α_{11}	-46970.6179	-46818.2988
α_{12}	121027.9850	121147.5239
α_{13}	-116852.3143	-116503.4214
α_{14}	40090.8675	39426.6000
α_{20}	-1992.6049	-1918.5814
α_{21}	34035.1117	33958.7106
α_{22}	-88551.1560	-88911.1854
α_{23}	86280.9477	86331.6192
α_{24}	-29898.3598	-29452.3086
α_{30}	415.2391	392.8688
α_{31}	-7149.5304	-7078.0582
α_{32}	18680.3346	18701.2904
α_{33}	-18292.8267	-18334.6005
α_{34}	6379.6448	6321.4971
β_{10}	367.8286	388.8533
β_{11}	-1213.7813	-1390.9306
β_{12}	1123.3026	1547.2662
β_{13}	-199.4380	-475.1178
γ_1	−0.00017	0.00034
γ_2	0.00294	0.00229
AAD	0.03 %	0.02 %
MAD	0.2 %	0.1 %
Bias	0.0002	0.0004
σ/(kg·m^{-3})	0.4	0.3

Both $\dot{Q}_{base}$ and $\dot{Q}_{measured}$ are electric powers ($\dot{Q}$) calculated using Equation (6), combining Ohm's Law and Joule's Law.

$$\dot{Q} = \frac{V^2}{R}(\%pulse) \quad (6)$$

where V is a constant voltage, R is the resistance and $\%\ pulse$ is the controlled percentage of pulse width supplied by an arbitrary waveform

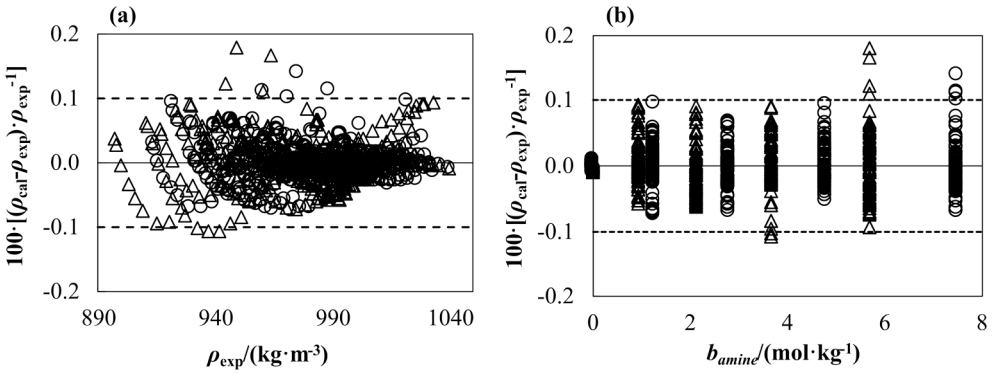

Fig. 5. Relative deviations (%) of experimental density measurements, ρ_{exp}, in comparison with calculated density, ρ_{cal}, using Equations 9 to 12. (a) Relative deviations vs ρ_{exp} and (b) Relative deviations vs b_{amine}. Mixtures: (△) DEAE + H_2O and (○) EAE + H_2O. Dotted lines represent the relative expanded uncertainty of our density measurements.

Table 6
Measurement conditions of literature data used to compare the experimental density measured in this work.

Literature	System	Densimeter	Conditions	Uncertainty[a]
Karunarathne et al. [27]	DEAE (1) + H_2O(2)	Anton Paar DMA-4500	w_1 = 0.30; 0.40 T = (293.15–353.15) K p = 0.1 MPa	1 %
Lebrette et al. [40]		Anton Paar DMA45	w_1 = 0.10; 0.20; 0.29; 0.39 T = (313.15–353.15) K p = 0.1 MPa	N.A.[b]
Pandey & Mondal [28]	EAE(1) + H_2O (2)	Anton Paar DMA 35	w_1 = 0.10; 0.20; 0.30 T = (293.15–333.15) K p = 0.1 MPa	0.3 %
Viet et al. [29]		Stabinger-type kinematic viscometer (SVM 3001, Anton Paar)	w_1 = 0.20; 0.40 T = (293.15–313.15) K p = 0.1 MPa	0.4 %

[a] Relative expanded uncertainty (k = 2), %.
[b] Not Available.

generator.

Friction along the tube causes a pressure loss and therefore the process is not isobaric. Furthermore, viscous dissipation implies heat that should be accounted for. Since the viscosities of the fluids used in this study are not high (less than 10 mPa·s) and the flow regime is laminar, the Poiseuille Law Equation (7) was applied to correct this effect and to determine the dissipative energy loss ($\dot{Q}_{correction}$). The magnitude of this correction is around 3 % in the final value of the isobaric heat capacity, which is higher than the uncertainty reported for the calorimeter. Consequently, the correction of viscosity in the isobaric heat capacity was taken into consideration.

$$\dot{Q}_{correction} = \frac{\dot{m}\Delta p}{\rho} = \frac{\dot{m}128L\eta\dot{v}}{\rho\pi D^4} = \frac{128L\eta\dot{v}^2}{\pi D^4} \tag{7}$$

where L is the tube length, D is the tube diameter, $\dot{v}$ is the volumetric flow rate, and η is the dynamic viscosity of the fluid at the calorimeter conditions. Equation (5) can be rewritten as Equation (8), adding the friction correction:

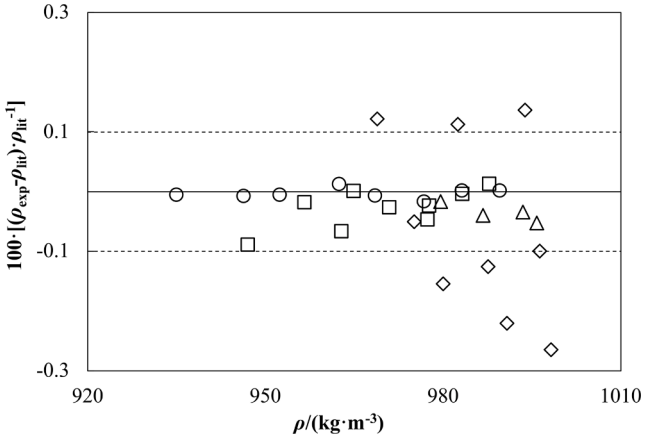

Fig. 6. Relative deviations (%) of density measurements, ρ_{exp}, in comparison with literature values, ρ_{lit}. Literature for DEAE + H_2O: (○) Karunarathne et al. [27] and (□) Lebrette et al. [40], and for EAE + H_2O: (◇) Pandey & Mondal [28] and (△) Viet et al. [29]. Dotted lines represent the relative expanded uncertainty of our density measurements.

$$\dot{Q}_{net} = \left[a + b\left(\dot{Q}_{base} - \dot{Q}_{measured}\right)\right] - \dot{Q}_{correction} \tag{8}$$

Viscosity is then a necessary input in the friction correction term. Some authors have reported viscosity measurements of aqueous amine mixtures. Maham et al. [26] and Karunarathne et al. [27] studied the viscosity of the DEAE + H_2O mixture, while Pandey & Mondal [28] and Viet et al. [29] measured the viscosities of EAE + H_2O mixture. Those experimental data were measured at atmospheric pressure, temperatures from (293.15 to 353.15) K and amine mass fractions of 0.1; 0.2; 0.3 and 0.4. High-pressure viscosity estimation was deemed unnecessary due to the negligible error introduced by using ambient-pressure viscosity. This error introduced to the isobaric heat capacity is only 0.03 % for the largest viscosity correction at the highest flow rate. This value is nearly an order of magnitude lower than the reported uncertainty.

3. Results and discussion

3.1. Density measurement

Density measurements of DEAE(aq) and EAE(aq) solutions were performed at pressures from (0.1 to 100) MPa and six temperatures from (293.15 to 393.15) K, for four amine mass fractions from 0.1 to 0.4. Mixtures are not liquid at temperatures above or equal to 373.15 K at

Table 7
Experimental isobaric heat capacity, c_p/(kJ·kg^{-1}·K^{-1}), for DEAE(1) + H_2O(2) mixture at different conditions of temperature, T, pressure, p, and amine mass fraction, w_1.[a]

	c_p/(kJ·kg^{-1}·K^{-1})			
	T/K			
p/MPa	293.15	313.15	333.15	353.15
	$w_1 = 0.100$			
0.1	4.22	4.21	4.23	4.19
5	4.22	4.21	4.22	4.19
10	4.18	4.19	4.20	4.20
15	4.18	4.20	4.21	4.18
20	4.17	4.19	4.21	4.18
25	4.16	4.18	4.22	4.18
	$w_1 = 0.200$			
0.1	4.24	4.19	4.23	4.23
5	4.28	4.19	4.21	4.22
10	4.26	4.17	4.19	4.22
15	4.26	4.23	4.19	4.24
20	4.24	4.20	4.20	4.23
25	4.26	4.18	4.21	4.23
	$w_1 = 0.300$			
0.1	4.14	4.11	4.13	4.20
5	4.12	4.13	4.11	4.15
10	4.12	4.13	4.10	4.13
15	4.13	4.10	4.10	4.18
20	4.13	4.11	4.11	4.16
25	4.17	4.12	4.12	4.10
	$w_1 = 0.400$			
0.1	3.96	4.00	4.02	4.09
5	3.92	3.96	4.02	4.07
10	3.94	3.95	4.01	4.04
15	3.91	3.97	4.00	4.05
20	3.89	3.97	4.04	4.07
25	3.85	3.99	4.01	4.07

[a]Expanded uncertainties ($k = 2$): $U(T) = 0.02$ K; $U_r(p) = 0.0005$; $U_r(w) = 0.0004$; $U_r(c_p) = 0.01$.

Table 8
Experimental isobaric heat capacity, c_p/(kJ·kg^{-1}·K^{-1}), for EAE(1) + H_2O(2) mixture at different conditions of temperature, T, pressure, p, and amine mass fraction, w_1.[a]

	c_p/(kJ·kg^{-1}·K^{-1})			
	T/K			
p/MPa	293.15	313.15	333.15	353.15
	$w_1 = 0.100$			
0.1	4.23	4.19	4.22	4.26
5	4.18	4.18	4.21	4.25
10	4.23	4.19	4.19	4.23
15	4.24	4.15	4.19	4.24
20	4.22	4.15	4.21	4.22
25	4.21	4.15	4.20	4.24
	$w_1 = 0.200$			
0.1	4.18	4.18	4.23	4.26
5	4.19	4.18	4.23	4.25
10	4.15	4.17	4.23	4.26
15	4.20	4.17	4.22	4.25
20	4.20	4.17	4.22	4.28
25	4.15	4.19	4.22	4.25
	$w_1 = 0.300$			
0.1	4.11	4.12	4.18	4.21
5	4.09	4.10	4.17	4.20
10	4.10	4.09	4.15	4.20
15	4.08	4.10	4.16	4.19
20	4.09	4.09	4.17	4.20
25	4.13	4.10	4.17	4.22
	$w_1 = 0.400$			
0.1	3.97	4.00	4.06	4.12
5	3.98	3.94	4.04	4.11
10	3.98	3.99	4.06	4.08
15	3.96	3.96	4.06	4.08
20	3.97	3.97	4.05	4.09
25	3.99	3.96	4.06	4.10

[a]Expanded uncertainties ($k = 2$): $U(T) = 0.02$ K; $U_r(p) = 0.0005$; $U_r(w) = 0.0004$; $U_r(c_p) = 0.01$.

atmospheric pressure, hence experimental data at 373.15 K and 393.15 K were gathered at pressures above 1 MPa. The experimental results are detailed in Table 2 for DEAE + H_2O and Table 3 for EAE + H_2O mixtures.

The experimental density data as a function of pressure at different temperatures are plotted in Fig. 3 for DEAE + H_2O and EAE + H_2O systems. Experimental data revealed that the densities of aqueous solutions containing EAE are slightly higher than those of the DEAE + H_2O mixture under identical conditions. This difference increases with both the mass fraction of amines and temperature, reaching a maximum of 1.5 % under these specified conditions. Although pure EAE has a higher density than pure DEAE, the molecular interaction between DEAE and H_2O reflects the compactness of the mixture due to a strong hydrogen bonding interaction [30]. This is caused by the capacity of DEAE to attract hydrogen and the donor ability of H_2O. On the other hand, EAE cannot form strong hydrogen bonds in the interaction with H_2O because this molecule is a secondary amine, and it can donate hydrogen rather than accept it [31]. As a result, the compactness of the EAE + H_2O molecule is lower than DEAE + H_2O. This may explain why EAE + H_2O has a higher density than DEAE + H_2O, keeping a fixed mass.

The density of these mixtures increases with pressure and decreases with temperature maintaining very similar trends for both mixtures, as can be seen in Fig. 3. Fig. 4 illustrates that as the amine mass fraction increases, the density of these mixtures decreases. This effect is more noticeable in the DEAE + H_2O system. It is important to note that not all the amine aqueous solutions show this performance. Mixtures like methyldiethanolamine (MDEA) + H_2O, monoethanolamine (MEA) + H_2O, diethanolamine (DEA) + H_2O and triethanolamine (TEA) + H_2O exhibit an increase in density with the rise of amine mass fraction, while 2-(dimethylamino)ethanol (DMEA) + H_2O shows the opposite effect [32,33].

The experimental density was correlated using a Tammann–Tait equation of state [35] that was modified to render density as a function of temperature, pressure, and molality, i.e., moles of amine divided by mass in kilograms of water (Equations 9 to 12). These equations replicate the density correlation model for brines as proposed by Al Ghafri et al. [36,37]. The reference density, ρ_{ref}, is computed with Equation (10) where $\rho_0(T)$ is the saturated liquid water density at the vapor pressure of pure water at the given temperature. The vapor pressure and the density of water are obtained from NIST REFPROP database [34].

$$\rho(T,p,b) = \frac{\rho_{ref}(T,b)}{1 - C(b)\ln\left(\frac{B(T,b)+p}{B(T,b)+p_{ref}(T)}\right)} \tag{9}$$

$$[\rho_{ref}(T,b) - \rho_0(T)]/\left(\mathrm{kg{\cdot}m^{-3}}\right) = \sum_{i=1}^{i=3} \alpha_{i0}\left[b/\left(\mathrm{mol{\cdot}kg^{-1}}\right)\right]^{(i+1)/2} + \sum_{i=1}^{i=3} \times \sum_{j=1}^{j=4} \alpha_{ij}\left[b/\left(\mathrm{mol{\cdot}kg^{-1}}\right)\right]^{(i+1)/2} (T/T_c)^{(j+1)/2} \tag{10}$$

$$B(T,b)\Big/\mathrm{MPa} = \sum_{i=0}^{i=1}\sum_{j=0}^{j=3} \beta_{ij}\left[b/\left(\mathrm{mol{\cdot}kg^{-1}}\right)\right]^{i} (T/T_c)^{j} \tag{11}$$

$$C(b) = \gamma_0 + \gamma_1\left[b/\left(\mathrm{mol{\cdot}kg^{-1}}\right)\right] + \gamma_2\left[b/\left(\mathrm{mol{\cdot}kg^{-1}}\right)\right]^{3/2} \tag{12}$$

The critical temperature, T_c, was 647.10 K in Equations (10) and (11). Firstly, the coefficients β_{0j}, and γ_0 in Equations (11) and (12) for pure water ($b_1 = 0$ mol·kg^{-1}) were determined. Table 4 provides these coefficients, which are identical for both aqueous amine solutions. The fit

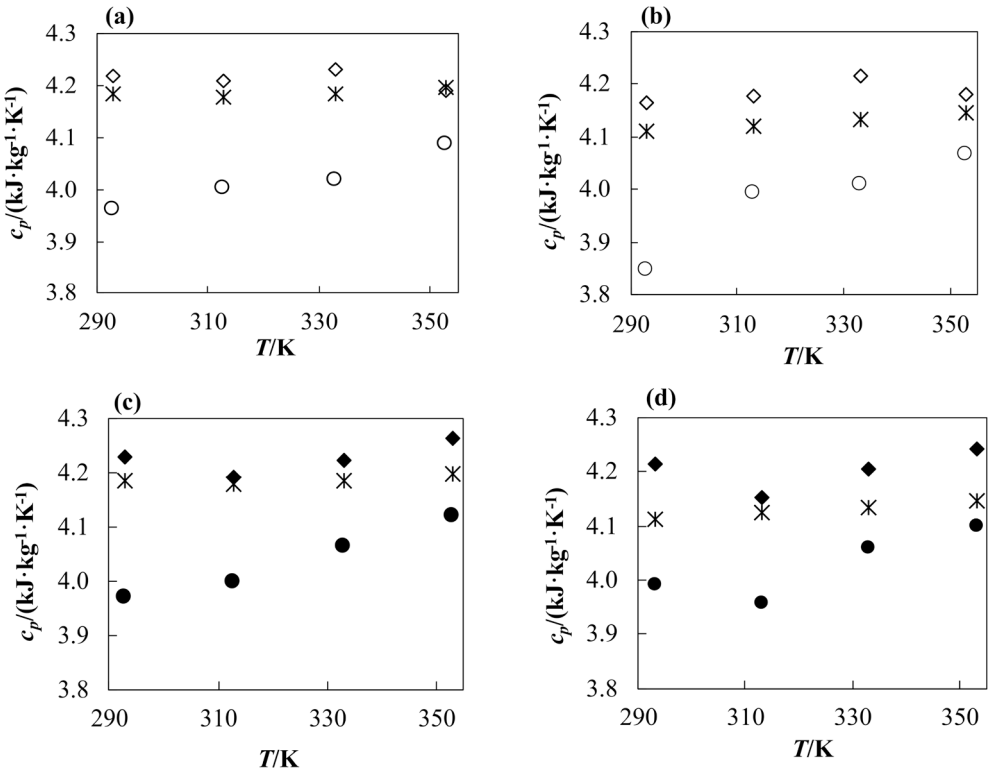

Fig. 7. Experimental isobaric heat capacity, c_p, as a function of temperature of the system: (a) DEAE + H_2O at $p = 0.1$ MPa, (b) DEAE + H_2O at $p = 25$ MPa, (c) EAE + H_2O at $p = 0.1$ MPa, and (d) EAE + H_2O at $p = 25$ MPa. Amine mass fraction: (*) $w_{amine} = 0$; (◇) $w_{DEAE} = 0.1$; (○) $w_{DEAE} = 0.4$; (◆) $w_{EAE} = 0.1$; (●) $w_{EAE} = 0.4$. Data for water from NIST REFPROP database [34].

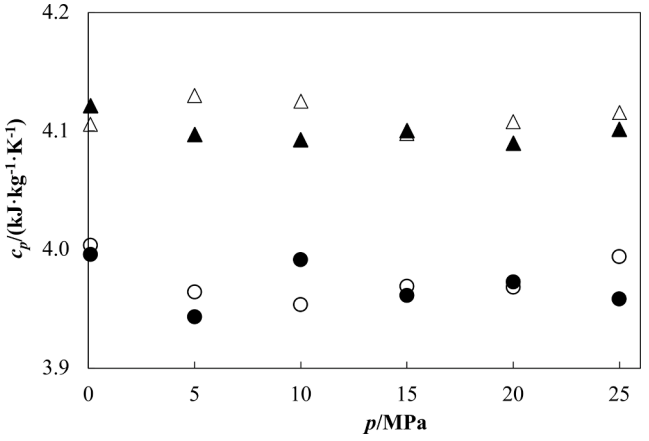

Fig. 8. Experimental isobaric heat capacity, c_p, at a temperature of 313.15 K as a function of pressure and amine mass fraction: (△) $w_{DEAE} = 0.3$; (○) $w_{DEAE} = 0.4$; (▲) $w_{EAE} = 0.3$; (●) $w_{EAE} = 0.4$.

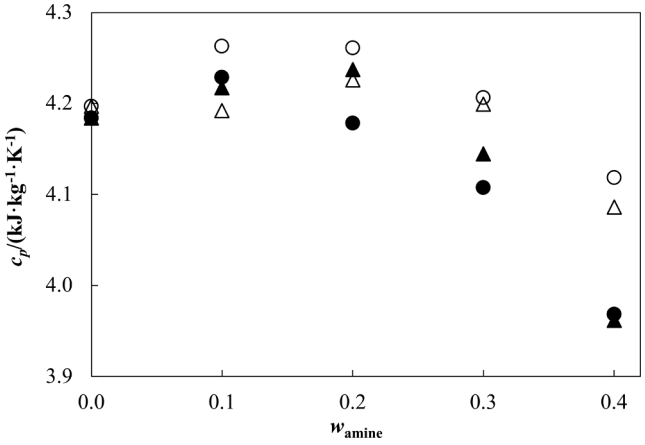

Fig. 9. Experimental isobaric heat capacity, c_p, at $p = 0.1$ MPa as a function of amine mass fraction, w_{amine}. (▲) DEAE + H_2O at 293.15 K, (△) DEAE + H_2O at 353.15 K, (●) EAE + H_2O at 293.15 K, and (○) EAE + H_2O at 353.15 K. Data for water from NIST REFPROP database [34].

resulted in density relative deviations for pure water below 0.01 %.

Then, the remaining coefficients in ρ_{ref}, B and C in Equations (10), 11 and 12 were optimized. The coefficients α_{ij}, β_{ij}, and γ_i are given in Table 5. Both fittings were carried out in MATLAB R2023b [38] by minimizing the sum of the squares of the differences between the experimental and calculated density values implementing a Levenberg-Marquardt algorithm [39]. Density measurements were fitted to a 26-parameter correlation model in both DEAE + H_2O and EAE + H_2O systems.

The modified correlation satisfactorily represents of the density over the entire range of temperature, pressure, and molality. Table 5 shows the fitting parameters and the absolute average relative deviation (AAD) using Equation (13), the average relative deviation (Bias) using Equation (14), the maximum absolute relative deviation (MAD) using Equation (15) and the standard deviation (σ) using Equation (16). Fig. 5 show the residuals of the fit. They agree with the density uncertainty, exhibiting no systematic trend in either molality or density.

$$\mathrm{AAD}, X = \frac{1}{N}\sum_{i=1}^{N}\frac{|X_{exp,i} - X_{cal,i}|}{X_{exp,i}} \tag{13}$$

$$\mathrm{MAD}, X = \max\left(\frac{|X_{exp,i} - X_{cal,i}|}{X_{exp,i}}\right) \tag{14}$$

Table 9
Fitting parameters of Equations (17) and (18) for correlations of DEAE + H_2O and EAE + H_2O isobaric heat capacity and average absolute relative deviations (AAD), maximum absolute relative deviation (MAD) and standard deviation (σ).

Parameters	Systems	
	DEAE + H_2O	EAE + H_2O
k_{11}	4.1158	4.1158
k_{12}	2.7041	-1.0216
k_{13}	-11.4458	-3.0864
k_{21}	$2.1821 \cdot 10^{-4}$	$2.1821 \cdot 10^{-4}$
k_{22}	$-6.2739 \cdot 10^{-3}$	$5.2387 \cdot 10^{-3}$
k_{23}	$2.6959 \cdot 10^{-2}$	$1.4666 \cdot 10^{-3}$
AAD	0.4 %	0.2 %
MAD	0.8 %	0.6 %
σ/(kJ·kg^{-1}·K^{-1})	0.02	0.01

$$\text{Bias}, X = \frac{1}{N}\sum_{i=1}^{N}\frac{X_{\text{exp,i}} - X_{\text{cal,i}}}{X_{\text{exp,i}}} \tag{15}$$

$$\sigma = \sqrt{\left[\frac{1}{N-m}\right]\sum_{i=1}^{N}\left(X_{\text{exp,i}} - X_{\text{cal,i}}\right)^2} \tag{16}$$

where $X_{\text{exp,i}}$ is the ith experimental value of a defined property X , $X_{\text{cal,i}}$ is the ith calculated value using the correlation at the same condition, N is the total number of experimental points, and m is the number of fitting parameters.

A literature search was carried out to compare our density experimental data. A review of the found experimental literature data is given in Table 6. Relative deviations of our measurements and literature values are plotted in Fig. 6 for DEAE + H_2O and EAE + H_2O mixtures.

All density data found in the literature were measured at atmospheric pressure and temperatures below 353.15 K. For aqueous solutions of DEAE, Karunarathne et al. [27] report eight common data points for comparison, with relative deviation within the uncertainty of our measurements. Lebrette et al. [40] published twelve common data points and all of them are consistent with our uncertainty.

Regarding EAE aqueous solutions, Fig. 6 shows a comparison with experimental data reported by Viet et al. [29] and by Pandey & Mondal [28]. For Viet et al. [29] we found an average relative deviation better than 0.04 % in agreement with our uncertainty. Pandey & Mondal [28] report nine common data points for comparison with a claimed relative uncertainty of 0.3 %. Deviations are within their experimental uncertainty.

3.2. Isobaric heat capacity measurement

Isobaric heat capacities were measured at four temperatures from 293.15 K up to 353.15 K, six pressures up to 25 MPa and amine mass fractions, w_1, of 0.1; 0.2; 0.3 and 0.4. The experimental values are shown in Tables 7 and 8, for DEAE + H_2O and EAE + H_2O systems respectively.

To investigate the influence of temperature, pressure, and amine mass fraction on isobaric heat capacities, experimental data for both systems were plotted as a function of temperature at a fixed pressure (Fig. 7), as a function of pressure at a fixed temperature (313.15 K) with different amine mass fractions (Fig. 8) and finally, as a function of amine mass fraction at atmospheric pressure (Fig. 9). Poling et al. [41] suggest that, at a reduced temperature below 0.7, there is not a strong dependence on temperature for liquid heat capacity. This is valid for the reduced range of temperatures that we studied for both mixtures. In Fig. 7 can be noticed that isobaric heat capacity increases an average of 3.8 % from (293.15 to 353.15) K in DEAE + H_2O mixture for w_{DEAE} = 0.4. Whereas, for EAE + H_2O mixture, an average rise of 1.9 %, 2.5 %, and 3.0 % were detected for w_{EAE} = 0.2, 0.3 and 0.4, respectively. This behavior agrees with the fact that temperature influences on the isobaric heat capacity of pure amines [42–44]. For the rest of the amine mass fractions, the change of c_p as a function of temperature is less than uncertainty. EAE aqueous solutions showed a minimum in c_p when w_{amine} = 0.1 at temperature of 313.15 K. In addition, aqueous solutions of DEAE presented this behaviour at w_{DEAE} = 0.2 and 0.3, at the same temperature. Aqueous solutions of amines studied in [25] also exhibited this performance.

The effect of pressure on these mixtures is shown in Fig. 8. For DEAE + H_2O system a decrease of 2.3 % can be noticed for w_{DEAE} = 0.3 at 353.15 K, and 2.8 % for w_{DEAE} = 0.4 at 293.15 K. For the rest of the amine mass fraction and temperature conditions, the change of c_p with pressure is below the uncertainty.

When amine mass fraction increases, isobaric heat capacity decreases at the same conditions of temperature and pressure when w_{amine} is higher than 0.1, as can be seen in Fig. 9. Isobaric heat capacity decreases an average of 4.9 % for DEAE + H_2O mixture, and 4.4 % for EAE + H_2O mixture.

Experimental data indicated that the isobaric heat capacities of both amine aqueous solutions are undistinguishable within the experimental uncertainty. DEAE + H_2O and EAE + H_2O isobaric heat capacities decrease with the mass fraction of amines and increase with temperature at the reported measuring conditions.

Isobaric heat capacities were correlated with temperature and amine mass fraction using an empirical correlation Equation (17) proposed by Al-Ghawas et al. [45].

$$c_p = K_1 + K_2 T \tag{17}$$

$$K_i = k_{i,1} + k_{i,2} w_1 + k_{i,3} {w_1}^2 \tag{18}$$

where K_1 and K_2 are two parameters calculated by Equation (18) using

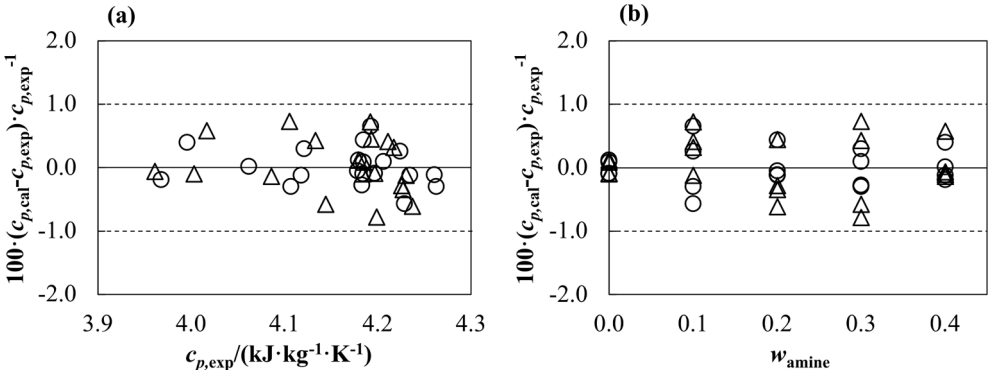

Fig. 10. Relative deviations (%) of isobaric heat capacity, $c_{p,\text{exp}}$, in comparison with calculated isobaric heat capacity, $c_{p,\text{cal}}$, using Equations (17) and (18). (a) Relative deviations vs $c_{p,\text{exp}}$ and (b) Relative deviations vs w_{amine}. Mixtures: (△) DEAE + H_2O and (○)-EAE + H_2O. Dotted lines represent the relative expanded uncertainty of our measurements.

$k_{i,1}$, $k_{i,2}$ and $k_{i,3}$ values; T is the temperature in Kelvin and, w_1 is the amine mass fraction.

Fitting parameters determined in Equations (17) and (18) are given in Table 9 for both systems of aqueous solutions of amine. Fig. 10 shows relative deviations between experimental isobaric heat capacities ($c_{p,exp}$) and the calculated values from the correlation model ($c_{p,cal}$). The average absolute relative deviations (AAD), the maximum absolute relative deviation (MAD) and the standard deviation (σ) were calculated using Equations (13), 14 and 15, respectively. These statistics are in good agreement with the uncertainty of our flow calorimeter.

Only one reference in the literature was found that provides experimental data on isobaric heat capacity for both systems. This property is reported by Cabani et al. [46] in the form of apparent molal heat capacity on a molality basis per gram of water ($J{\cdot}mol^{-1}{\cdot}K^{-1}$). The average value of apparent molal heat capacity, Φ_{c_p}, at 313.15 K for a molal concentration range between (0.35 and 0.99) $mol{\cdot}kg^{-1}$ is 540 ±8 $J{\cdot}mol^{-1}{\cdot}K^{-1}$ for DEAE + H_2O. The average value is 391 ±10 $J{\cdot}mol^{-1}{\cdot}K^{-1}$ for EAE + H_2O in a molal concentration range between (0.36 and 0.98) $mol{\cdot}kg^{-1}$. Our experimental isobaric heat capacity data were converted to units of apparent molal heat capacity ($J{\cdot}mol^{-1}{\cdot}K^{-1}$) using Equation (19), as proposed by the same research group in a prior publication [47].

$$\Phi_{c_p} = \left(\frac{1}{b_1} + M_1\right) c_p - \frac{1}{b_1} c_{p,w} \tag{19}$$

where M_1 is the amine molar mass, b_1 is the molality of the amine aqueous solution, and $c_{p,w}$ is the water specific isobaric heat capacity at a given temperature. The latter was obtained from NIST REFPROP database [34].

Upon conversions, relative deviations of 3 % for DEAE + H_2O and 2 % for EAE + H_2O, corresponding to apparent molal heat capacities of 525 $J{\cdot}mol^{-1}{\cdot}K^{-1}$ (4.21 $kJ{\cdot}kg^{-1}{\cdot}K^{-1}$ at amine mass fraction of 0.1, atmospheric pressure and 313.15 K) and 382 $J{\cdot}mol^{-1}{\cdot}K^{-1}$ (4.19 $kJ{\cdot}kg^{-1}{\cdot}K^{-1}$ at amine mass fraction of 0.1, atmospheric pressure and 313.15 K), respectively, were found. These deviations are considered acceptable, given the expected uncertainties and that the reported apparent molal heat capacity represents an average value across a range of molal concentrations.

4. Conclusions

Density and isobaric heat capacity measurements of DEAE + H_2O and EAE + H_2O mixtures (amine mass fraction: 0.1; 0.2; 0.3 and 0.4) were carried out at wide pressure and temperature ranges. A vibrating tube densimeter was used for density measurement with a relative expanded uncertainty of ±0.1 % ($k = 2$) and a flow calorimeter for isobaric heat capacity measurements with a relative expanded uncertainty of ±1 % ($k = 2$).

Density data in both aqueous solutions show similar behavior in terms of the effect of temperature, pressure, and amine mass fraction: density increases when pressure increases; density increases when temperature and amine mass fraction decrease. Experiments revealed that the densities of aqueous solutions containing EAE are slightly higher than those of the DEAE + H_2O mixture under identical conditions. This difference increases with both the mass fraction of amines and temperature. These trends pertain to these systems but may not be equal to other amines in aqueous solutions or thermodynamic states. Comparison with literature is in good agreement with the reported uncertainties.

A modified Tammann-Tait Equation of State, including the molality dependence, proved to be adequate for correlating experimental density data concerning pressure and temperature. This model achieved good absolute average relative deviations (AAD ≤ 0.03 %) compared with the experimental density. We have demonstrated the suitability of molality units for accurately deriving empirical correlations of density in various amine aqueous solutions rather than mass or mole fractions. Furthermore, the modified Tammann-Tait equation, originally proposed by Al Ghafri et al. for brine densities [36,37], has also proven effective in correlating densities of binary amine + H_2O systems. In future works, we will show that the same equation of state can effectively fit density data for ternary CO_2 + amine + H_2O mixtures.

Isobaric heat capacities are not strongly influenced by temperature or pressure; however, an increase in amine mass fraction leads to a decline in this property. DEAE + H_2O and EAE + H_2O isobaric heat capacities are indistinguishable within the experimental uncertainty. An empirical correlation proposed for isobaric heat capacity data was fitted as a function of temperature and amine mass fraction (AAD ≤ 0.04 %). Our experimental results demonstrated good agreement with the experimental data reported in the available literature.

CRediT authorship contribution statement

Yisel Pérez-Milian: Writing – review & editing, Writing – original draft, Investigation, Formal analysis, Data curation. **Alejandro Moreau:** Writing – review & editing, Validation, Supervision, Methodology, Investigation, Formal analysis, Data curation, Conceptualization. **Juan D. Arroyave:** Writing – review & editing, Formal analysis, Data curation. **Fredy Vélez:** Writing – review & editing, Validation, Formal analysis. **Xavier Paredes:** Validation, Resources, Methodology, Formal analysis. **David Vega-Maza:** Writing – review & editing, Supervision, Methodology, Funding acquisition, Conceptualization.

Declaration of competing interest

The authors declare that they have no known competing financial interests or personal relationships that could have appeared to influence the work reported in this paper.

Data availability

Data will be made available on request.

Acknowledgments

Project “CLU-2019-04 – BIOECOUVA Unit of Excellence ” of the University of Valladolid, funded by the Junta de Castilla y León and co-financed by the European Commission (ERDF “Europe drives our growth”). Y.P.M. and J.D.A. have been funded by the call for predoctoral contracts UVa 2021, co-funded by Banco Santander. D.V.M. acknowledges his “Beatriz Galindo Senior” fellowship BEAGAL18/00259.

References

[1] IPCC. The Physical Science Basis, Cambridge University Press, Cambridge, United Kingdom and New York, NY, USA, 2021. https://www.ipcc.ch/report/sixth-assessment-report-working-group-i/.
[2] IPCC. Mitigation of Climate Change, Cambridge University Press, Cambridge, UK and New York, NY, USA, 2022. https://www.ipcc.ch/report/sixth-assessment-report-working-group-3/.
[3] IPCC. Renewable Energy Sources and Climate Change Mitigation, Cambridge University Press, Cambridge, United Kingdom and New York, NY, USA, 2011, p. 1075. https://www.ipcc.ch/report/renewable-energy-sources-and-climate-change-mitigation/.
[4] IPCC. Carbon Dioxide Capture and Storage, Cambridge University Press, UK, 2005, p. 43. https://www.ipcc.ch/report/carbon-dioxide-capture-and-storage/.
[5] A.L. Kohl, R.B. Nielsen, Gas Purification, 5th ed., Gulf Publishing Co., Houston, TX, 1997.
[6] D. Aaron, C. Tsouris, Separation of CO_2 from flue gas: A review, Sep Sci Technol 40 (2005) 321–348, https://doi.org/10.1081/SS-200042244.
[7] M.E. Boot-Handford, J.C. Abanades, E.J. Anthony, M.J. Blunt, S. Brandani, N. Mac Dowell, J.R. Fernández, M.C. Ferrari, R. Gross, J.P. Hallett, R.S. Haszeldine, P. Heptonstall, A. Lyngfelt, Z. Makuch, E. Mangano, R.T.J. Porter, M. Pourkashanian, G.T. Rochelle, N. Shah, J.G. Yao, P.S. Fennell, Carbon capture and storage update, Energy Environ Sci 7 (2014) 130–189, https://doi.org/10.1039/c3ee42350f.
[8] N. MacDowell, N. Florin, A. Buchard, J. Hallett, A. Galindo, G. Jackson, C. S. Adjiman, C.K. Williams, N. Shah, P. Fennell, An overview of CO_2 capture

technologies, Energy Environ Sci 3 (2010) 1645–1669, https://doi.org/10.1039/c004106h.
[9] R.K. Abdulrahman, I.M. Sebastine, Natural gas sweetening process simulation and optimization: A case study of Khurmala field in Iraqi Kurdistan region, J Nat Gas Sci Eng 14 (2013) 116–120, https://doi.org/10.1016/j.jngse.2013.06.005.
[10] R.L. Casselman, Sour-Gas Sweetening During Offshore Drillstem Tests-A Case History, SPE Prod. Eng. (1990) 103–106.
[11] H. Li, B. Dong, Z. Yu, J. Yan, K. Zhu, Thermo-physical properties of CO_2 mixtures and their impacts on CO_2 capture, transport and storage: Progress since 2011, Appl Energy 255 (2019), https://doi.org/10.1016/j.apenergy.2019.113789.
[12] J.-C. De Hemptinne, G.M. Kontogeorgis, R. Dohrn, I.G. Economou, A. Ten, K. S. Kuitunen, L. Fele, Z. Ilnik, M.G. De Angelis, V. Vesovic, A View on the Future of Applied Thermodynamics, Ind Eng Chem Res 61 (2022), https://doi.org/10.1021/acs.iecr.2c01906.
[13] F. Meng, Y. Meng, T. Ju, S. Han, L. Lin, J. Jiang, Research progress of aqueous amine solution for CO2 capture: A review, Renew. Sustain. Energy Rev. 168 (2022) 112902, https://doi.org/10.1016/J.RSER.2022.112902.
[14] S.S. Karunarathne, D.A. Eimer, L.E. Øi, Physical Properties of MEA + Water + CO_2 Mixtures in Postcombustion CO_2 Capture: A Review of Correlations and Experimental Studies, J. Eng. (United Kingdom) (2020), https://doi.org/10.1155/2020/7051368.
[15] F.A. Chowdhury, H. Yamada, T. Higashii, K. Goto, M. Onoda, CO_2 Capture by Tertiary Amine Absorbents: A Performance Comparison Study, Ind Eng Chem Res 52 (2013) 8323–8331, https://doi.org/10.1021/ie400825u.
[16] D. Tong, J.P.M. Trusler, G.C. Maitland, J. Gibbins, P.S. Fennell, Solubility of carbon dioxide in aqueous solution of monoethanolamine or 2-amino-2-methyl-1-propanol: Experimental measurements and modelling, Int. J. Greenhouse Gas Control 6 (2012) 37–47, https://doi.org/10.1016/j.ijggc.2011.11.005.
[17] N. El Hadri, D.V. Quang, E.L.V. Goetheer, M.R.M. Abu Zahra, Aqueous amine solution characterization for post-combustion CO_2 capture process, Appl Energy 185 (2017) 1433–1449, https://doi.org/10.1016/j.apenergy.2016.03.043.
[18] D. Vega-Maza, M. Carmen Martín, J.P. Martin Trusler, J.J. Segovia, Heat capacities and densities of the binary mixtures containing ethanol, cyclohexane or 1-hexene at high pressures, J. Chem. Thermodyn. 57 (2013) 550–557, https://doi.org/10.1016/j.jct.2012.07.018.
[19] J.J. Segovia, O. Fandiño, E.R. López, L. Lugo, M. Carmen Martín, J. Fernández, Automated densimetric system: Measurements and uncertainties for compressed fluids, J Chem Thermodyn 41 (2009) 632–638, https://doi.org/10.1016/J.JCT.2008.12.020.
[20] B. Lagourette, C. Boned, H. Saint-Guirons, P. Xans, H. Zhout, Densimeter calibration method versus temperature and pressure, Meas. Sci. Technol 3 (1992) 699–703.
[21] M.J.P. Comuñas, J.P. Bazile, A. Baylaucq, C. Boned, Density of diethyl adipate using a new vibrating tube densimeter from (293.15 to 403.15) K and up to 140 MPa calibration and measurements, J Chem Eng Data 53 (2008) 986–994, https://doi.org/10.1021/JE700737C.
[22] L. Lugo, M.J.P. Comuñas, E.R. López, J. Fernández, (p, Vm, T, x) measurements of dimethyl carbonate + octane binary mixtures I, Experimental Results, Isothermal Compressibilities, Isobaric Expansivities and Internal Pressures, Fluid Phase Equilib 186 (2001) 235–255.
[23] JCGM 100:2008, Evaluation of measurement data. Guide to the expression of uncertainty in measurement, (2008).
[24] J.J. Segovia, D. Vega-Maza, C.R. Chamorro, M.C. Martín, High-pressure isobaric heat capacities using a new flow calorimeter, J. Supercrit. Fluids 46 (2008) 258–264, https://doi.org/10.1016/J.SUPFLU.2008.01.011.
[25] E.I. Concepción, A. Moreau, D. Vega-Maza, X. Paredes, M.C. Martín, Heat capacities of different amine aqueous solutions at pressures up to 25 MPa for CO_2 capture, J Mol Liq 377 (2023) 121575, https://doi.org/10.1016/j.molliq.2023.121575.
[26] Y. Maham, L. Lebrette, A.E. Mather, Viscosities and Excess Properties of Aqueous Solutions of Mono and Diethylethanolamines at Temperatures between 298.15 and 353.15 K, J. Chem. Eng. Data 47 (2002) 550–553, https://doi.org/10.1021/je015528d.
[27] S.S. Karunarathne, D.A. Eimer, L.E. Øi, Density, Viscosity, and Excess Properties of MDEA + H_2O, DMEA + H_2O, and DEEA + H_2O Mixtures, Appl. Sci 10 (2020) 3196, https://doi.org/10.3390/app10093196.
[28] D. Pandey, M.K. Mondal, Viscosity, density, and derived thermodynamic properties of aqueous 2-(ethylamino)ethanol (EAE), aqueous aminoethylethanolamine (AEEA), and its mixture for post-combustion CO_2 capture, J Mol Liq 332 (2021) 115873, https://doi.org/10.1016/J.MOLLIQ.2021.115873.
[29] K. Viet, B. Tran, M. Sato, K. Yanase, T. Yamaguchi, H. Machida, K. Norinaga, Density and Viscosity Calculation of a Quaternary System of amine absorbents before and after carbon dioxide absorption, J. Chem. Eng. Data 66 (2021) 3057–3071, https://doi.org/10.1021/acs.jced.1c00195.
[30] B. Hawrylak, S.E. Burke, R. Palepu, Partial Molar and Excess Volumes and Adiabatic Compressibilities of Binary Mixtures of Ethanolamines with Water, J Solution Chem 29 (2000).
[31] C. Zhu, X. Liu, T. Fu, X. Gao, Y. Ma, Density, viscosity and excess properties of N, N-dimethylethanolamine +2-(ethylamino) ethanol +H_2O at T = (293.15 to 333.15) K, J Mol Liq 319 (2020) 114095, https://doi.org/10.1016/J.MOLLIQ.2020.114095.
[32] M. Sobrino, E.I. Concepción, Á. Gómez-Hernández, M.C. Martín, J.J. Segovia, Viscosity and density measurements of aqueous amines at high pressures: MDEA-water and MEA-water mixtures for CO_2 capture, J Chem Thermodyn 98 (2016) 231–241, https://doi.org/10.1016/J.JCT.2016.03.021.
[33] E.I. Concepción, Á. Gómez-Hernández, M.C. Martín, J.J. Segovia, Density and viscosity measurements of aqueous amines at high pressures: DEA-water, DMAE-water and TEA-water mixtures, J Chem Thermodyn 112 (2017) 227–239, https://doi.org/10.1016/J.JCT.2017.05.001.
[34] E.W. Lemmon, I.H. Bell, M.L. Huber, M.O. McLinden, NIST Standard Reference Database 23: Reference Fluid Thermodynamic and Transport Properties-REFPROP, Version 10.0, 2018, National Institute of Standards and Technology, Standard Reference Data Program Gaithersburg, http://doi.org/10.18434/T4/1502528.
[35] J.H. Dymond, R. Malhotra, The Tait Equation: 100 Years On, Int J Thermophys 9 (1988).
[36] S. Al Ghafri, G.C. Maitland, J.P.M. Trusler, Densities of aqueous $MgCl_2$(aq), $CaCl_2$(aq), KI(aq), NaCl(aq), KCl(aq), $AlCl_3$(aq), and (0.964 NaCl + 0.136 KCl)(aq) at temperatures between (283 and 472) K, pressures up to 68.5 MPa, and molalities up to 6 mol·kg^{-1}, J. Chem. Eng. Data 57 (2012) 1288–1304, https://doi.org/10.1021/je2013704.
[37] S. Al Ghafri, G.C. Maitland, J.P.M. Trusler, Correction to "Densities of aqueous $MgCl_2$(aq), $CaCl_2$(aq), KI(aq), NaCl(aq), KCl(aq), $AlCl_3$(aq), and (0.964 NaCl + 0.136 KCl)(aq) at temperatures between (283 and 472) K, pressures up to 68.5 MPa, and molalities up to 6 mol·kg^{-1}, J. Chem. Eng. Data 64 (2019), https://doi.org/10.1021/acs.jced.9b00316, 2912–2912.
[38] The MathWorks Inc., MATLAB (R2023b), (2023). https://matlab.mathworks.com/ (accessed February 5, 2024).
[39] P.R. Bevington, D.K. Robinson, Data Reduction and Error Analysis for the Physical Sciences, McGraw-Hill, London, 1992.
[40] L. Lebrette, Y. Maham, T.T. Teng, L.G. Hepler, A.E. Mather, Volumetric properties of aqueous solutions of mono, and diethylethanolamines at temperatures from 5 to 80 °C II, Thermochim Acta 386 (2002) 119–126, https://doi.org/10.1016/S0040-6031(01)00813-9.
[41] B.E. Poling, J. ÓConnell, J.M. Prausnitz. The properties of gases and liquids, Fifth Edition, McGraw-Hill, 2001.
[42] B.P. Soares, V. Štejfa, O. Ferreira, S.P. Pinho, K. Růžička, M. Fulem, Vapor pressures and thermophysical properties of selected ethanolamines, Fluid Phase Equilibria 473 (2018) 245–254, https://doi.org/10.1016/J.FLUID.2018.05.032.
[43] A.V. Rayer, A. Henni, P. Tontiwachwuthikul, Molar heat capacities of solvents used in CO_2 capture: A group additivity and molecular connectivity analysis, Can. J. Chem. Eng. 90 (2012) 367–376, https://doi.org/10.1002/CJCE.20646.
[44] I.M.S. Lampreia, A.F.S. Santos, Ultrasound Speeds and Molar Isentropic Compressions of Aqueous 2-(Ethylamino)ethanol Mixtures from 283.15 to 303.15 K, J. Solution Chem. 39 (2010) 808–819, https://doi.org/10.1007/s10953-010-9546-5.
[45] H.A. Al-Ghawas, D.P. Hagewlesche, G. Rulz-Ibanez, O.C. Sandall, Physicochemical Properties Important for Carbon Dioxide Absorption in Aqueous Methyldiethanolamine, J. Chem. Eng. Data 34 (1989) 385–391, https://doi.org/10.1021/je00058a004.
[46] S. Cabani, S.T. Lobo, E. Matteo Ii, Apparent Molal Heat Capacities of Organic Solutes in Water. V. Aminoalcohols, Arninoethers, Diamines, and Polyethers, J Solution Chem 8 (1979) 5–10.
[47] S. Cabani, G. Conti, E. Matteoli, A. Tani, Apparent Molal Heat Capacities of Organic Compounds in Aqueous Solution, J. Chem. Soc., Faraday Trans. 1: Phys. Chem. Condensed Phases 73 (1977) 476–486, https://doi.org/10.1039/F19777300476.